Calculation of the weakly coupled 1 and 2 $^1\Pi$ twin states of KRb

Thierry Leininger and Gwang-Hi Jeung*
Laboratoire de Chimie Quantique, Institut Le Bel, Université Louis Pasteur, 4 rue Blaise Pascal, 67000 Strasbourg, France
(Received 25 February 1994)

Spectroscopic properties of all excited states of KRb dissociating into $4s(K)+5s(Rb)$, $4s(K)+5p(Rb)$, and $4p(K)+5s(Rb)$ are studied, using quantum chemical calculations. Only the 1 and 2 $^1\Pi$ states showed a weak coupling between the $4s(K)+5p(Rb)$ and the $4p(K)+5s(Rb)$ components. The dipole moments, atomic orbital populations, and transition dipole moments of those two states showed a twin nature. Calculated Einstein coefficients for the $1\,^1\Pi-X$ and $2\,^1\Pi-X$ dipole transitions predict unusually rich band spectra. The intensity distributions of those two transitions showed a remarkable difference.

PACS number(s): 31.20.Di, 31.50.+w, 33.10.Gx

I. INTRODUCTION

The electronic states of KRb are not well known among the alkali diatomic molecules. The ground-state characteristics were only very recently reported by Ross *et al.* [1], who analyzed laser-induced fluorescence spectra, $A\,^1\Sigma^+ \rightarrow X\,^1\Sigma^+$, to find the spectroscopic constants covering the ranges $0 \le v \le 44$ and $J \le 141$. Unresolved diffuse bands in the visible region originating from transitions between excited states have been reported by Beuc, Milosevic, and Pichler [2].

One aspect of the excited states of KRb is of particular interest, which is the energetic proximity of the dissociation channels $4s(K)+5p(Rb)$ and $4p(K)+5s(Rb)$. As the energy levels for these two channels are separated by only from 0.028 ($J=3/2$) to 0.050 eV ($J=1/2$) [3], one might expect a strong coupling between these two components (two nonorthogonal basis functions) in the pair of electronically excited states of the same symmetry dissociating into these two channels.

We performed quantum chemical calculations for the ground state and the excited electronic states dissociating into $4s(K)+5p(Rb)$ and $4p(K)+5s(Rb)$. The $2,3\,^1\Sigma^+$ pair, $2,3\,^3\Sigma^+$ pair, and $1,2\,^3\Pi$ pair states showed strong coupling between these two components and this coupling led to large energetic separations within each pair. Only the 1 and 2 $^1\Pi$ states, which will be simply referred to as $\underline{1}$ and $\underline{2}$ states hereafter, showed a weak coupling between these two components. In this paper, we report the spectroscopic constants of all electronic states dissociating into $4s(K)+5s(Rb)$, $4s(K)+5p(Rb)$, and $4p(K)+5s(Rb)$ and we analyze the $\underline{1}$ and $\underline{2}$ states in particular.

II. METHOD OF COMPUTATION

The small-core relativistic pseudopotentials of Christiansen and co-workers used to simulate the $[1s^2/2s^22p^6]$ core of the potassium atom [4] and the $[1s^2/2s^22p^6/3s^23p^63d^{10}]$ core of rubidium atom [5]. The restricted Hartree-Fock (RHF) calculations were done, using the ASTERIX program package [6]. The configuration-interaction (CI) calculation was done using a program originally written by Brooks and Schaefer [7] and a direct CI program with contractions by Siegbahn [8]. The molecular orbitals resulting from the RHF calculation of KRb^+ were employed as one-electron basis functions for CI calculations. Only the two valence electrons were correlated for the excited states, because the valence-core effect for the excited states is much smaller than for the ground state. The population analysis was done using the natural molecular orbitals resulting from the CI.

The $6s6p5d$ Gaussian-type orbitals (GTOs) to best describe the $4s$, $4p$, and $3d$ atomic states of potassium (and $5s$, $5p$, and $4d$ of rubidium) were obtained. Two s GTOs were added to describe the $(n+1)s$ state, and one diffuse p GTO and one diffuse d GTO were also added. These $8s7p6d$ GTOs were contracted to $7s6p4d$ atomic basis functions. Then one f GTO was added to each atom with exponents 1.119 (K) and 0.8075 (Rb). The $4s \rightarrow 4p$ (K) and $5s \rightarrow 5p$ (Rb) excitation energies calculated in the RHF approximation, valence-core CI, the nine-electron ($9e^-$) SDCI, and with Langhoff and Davidson's correction [9] are summarized in Table I. It shows the importance of the valence-core and core-core electron correlation effects for the atomic energies.

The static and transition dipole moments were calculated also using the CI wave functions. The nonadiabatic terms neglected in the Born-Oppenheimer approximation

$$\left\langle \Phi_m(R) \left| -\frac{\hbar^2}{2I}\frac{\partial}{\partial R}R^2\frac{\partial}{\partial R} \right| \Phi_n(R) \right\rangle ,$$

where Φ_m and Φ_n are the wave functions of electronic states and $I=\mu R^2$ is the moment of inertia of KRb, were calculated. The ground (X) state was calculated in a 14-electron CI including the $3p(K)$ and $4p(Rb)$ core electrons. Four configuration-state functions $(1\sigma)^2$, $(1\sigma^*)^2$, $(1\pi_x)^2$, and $(1\pi_y)^2$ were used as the zeroth-order reference. All single and double excitations from that refer-

*Corresponding author.

TABLE I. Calculated atomic excitation energies $4s \rightarrow 4p$ (K) and $5s \rightarrow 5p$ (Rb) in cm^{-1}.

	RHF	VCCI[a]	$9e^-$ SDCI	$+Q$[b]	Experimental $J=\frac{1}{2}$	Experimental $J=\frac{3}{2}$
K($4s \rightarrow 4p$)	11 462	12 626	12 696	12 800	12 985	13 043
Rb($5s \rightarrow 5p$)	10 833	12 204	12 252	12 381	12 579	12 817
ΔE[c]	629	422	444	419	406	226

[a]Valence-core correlation values.
[b]$9e^-$ SDCI with correlation energies according to Langhoff and Davidson [9].
[c]Energy difference between K($4p$)+Rb($5s$) and K($4s$)+(Rb)($5p$).

ence function were included in the CI. This multireference (MR) CI calculation gave $R_e = 4.06$ Å and $\omega_e = 70$ cm^{-1}, which are in fairly good agreement with the values of Ross *et al.*, $R_e = 4.0685$ Å and $\omega_e = 75.842$ cm^{-1}. The long-range part of the ground-state potential curve did not agree well with the RKR curve. This disagreement is due to a size-consistency problem of the MRCI. Comparing the molecular MRCI energies to the atomic MRCI energies gave a dissociation energy of 0.47 eV. It is coincidentally in perfect agreement with an experimental estimate obtained using negative ion photoelectron spectroscopy [10].

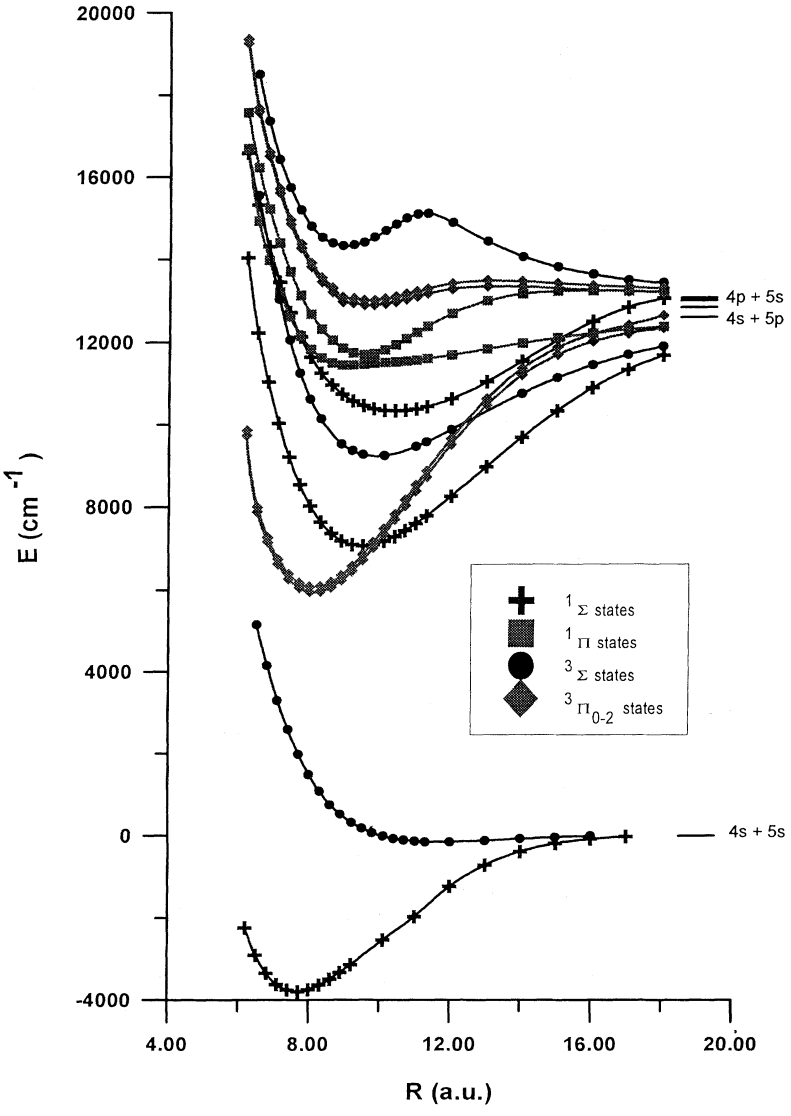

FIG. 1. Potential-energy curves for the electronic states of KRb dissociating into $4s$(K) $+5s$(Rb), $4s$(K)$+5p$(Rb), and $4p$(K)$+5s$(Rb).

TABLE II. Potential energies (cm^{-1}) of the electronic states of KRb.

R (bohrs)	$1\,^1\Sigma^+$	$2\,^1\Sigma^+$	$3\,^1\Sigma^+$	$1\,^3\Sigma^+$	$2\,^3\Sigma^+$	$3\,^3\Sigma^+$
6.2	−1769	14 036	16 571	6406	17 712	20 550
6.5	−2584	12 219	15 314	5155	15 546	18 489
6.8	−3162	11 030	14 302	4148		17 352
7.1	−3535	10 027	13 442	3294	13 020	16 414
7.4	−3735	9 199	12 717	2577	12 039	15 730
7.7	−3792	8 534	12 118	1977	11 240	15 188
8.0	−3735	8 018	11 633	1486	10 610	14 795
8.3	−3590	7 632	11 247	1089	10 125	14 532
8.6	−3381	7 360	10 950	768		14 381
8.9	−3126	7 184	10 727	516	9 515	14 319
9.2	−2843	7 092	10 562	320	9 350	14 335
9.5	−2546	7 066	10 450	171	9 256	14 409
9.8	−2247	7 097	10 375	59		14 530
10.1	−1953	7 171	10 334	−21	9 232	14 684
10.4	−1672	7 285	10 323	−79		14 842
10.7	−1410	7 426	10 334	−116		14 989
11.0	−1169	7 590	10 364	−140	9 449	15 087
11.3	−947	7 773	10 417	−154	9 561	15 103
11.65				−158	9 706	15 022
12.0	−700	8 242	10 608	−153	9 859	14 877
13.0	−414	8 958	11 019	−121		14 416
14.0	−223	9 664	11 521	−79	10 739	14 047
15.0	−113	10 312	12 032	−42	11 113	13 786
16.0	−50	10 869	12 478	−13	11 426	13 608
17.0	−14	11 317	12 816		11 679	13 487
18.0		11 659	13 033		11 878	13 406
∞	0	12 579	12 985	0	12 579	12 985

R (bohrs)	$1\,^1\Pi$	$2\,^1\Pi$	$1\,^3\Pi_0$	$1\,^3\Pi_2$	$2\,^3\Pi_0$	$2\,^3\Pi_2$
6.2	16 685	17 563	9 734	9 850	19 234	19 334
6.5	14 932	16 216	7 877	7 993	17 571	17 671
6.8	13 975	15 226	7 154	7 272	16 495	16 595
7.1	13 202	14 394	6 628	6 746	15 595	15 695
7.4	12 599	13 698	6 268	6 386	14 855	14 957
7.7	12 142	13 125	6 053	6 171	14 262	14 364
8.0	11 820	12 699	5 996	6 078	13 799	13 901
8.3	11 609	12 311	5 966	6 090	13 450	13 552
8.6	11 488	12 041	6 063	6 187	13 201	13 305
8.9	11 438	11 850	6 230	6 354	12 970	13 076
9.2	11 438	11 734	6 451	6 579	12 937	13 043
9.5	11 457	11 690	6 719	6 847	12 891	13 001
9.8	11 482	11 719	7 017	7 147	12 889	12 999
10.1	11 493	11 806	7 339	7 469	12 917	13 041
10.4	11 508	11 932	7 688	7 810	12 967	13 083
10.7	11 528	12 074	8 024	8 158	13 018	13 144
11.0	11 554	12 223	8 374	8 510	13 092	13 212
11.3	11 587	12 368	8 720	8 858	13 154	13 278
12.0	11 677	12 676	9 497	9 639	13 269	13 399
13.0	11 820	12 983	10 456	10 606	13 332	13 464
14.0	11 960	13 145	11 179	11 341	13 320	13 446
15.0	12 087	13 207	11 679	11 851	13 280	13 398
16.0	12 193	13 220	11 999	12 181	13 238	13 348
17.0	12 281	13 209	12 195	12 389	13 206	13 304
18.0	12 351	13 194	12 317	12 521	13 181	13 273
∞	12 579	12 985	12 579	12 817	12 985	13 043

The potential-energy curves, static dipole moment curves, and transition dipole moment curves were fitted with cubic spline functions to find equilibrium spectroscopic constants. The vibrational wave functions for the ground state were calculated using the Rydberg-Klein-Rees (RKR) potential curve of Ross *et al.* [1]. The products of the vibrational wave functions $W_{(m,v')}(R)$ and $W_{(n,v'')}(R)$ and the transition dipole moment as a function of the internuclear distance $\vec{\mu}_{(m\leftarrow n)}(R)$ were numerically integrated to obtain the vibronic transition dipole moment

$$p^{u}_{(mv'\leftarrow nv'')}=\int_0^\infty dR\; W^{*}_{(n,v'')}(R)W_{(m,v')}(R)\mu^{u}_{(m\leftarrow n)}(R)\ ,$$

where n and m designate the lower and the upper electronic states, respectively, v'' and v' designate the corresponding vibrational states, and u represents the x,y, and z components. Then the Einstein coefficients of stimulated absorption for vibronic transitions [11] were obtained according to

$$B_{(mv'\leftarrow nv'')}=\frac{\mu_0 c^2}{6\hbar^2}\sum_u\left|p^{u}_{(mv'\leftarrow nv'')}\right|^2 .$$

III. RESULTS AND DISCUSSION

The calculated potential-energy curves for the $1\,^{1,3}\Sigma^+$ states dissociating into $4s(\mathrm{K})+5s(\mathrm{Rb})$, the $2\,^{1,3}\Sigma^+$ and $1\,^{1,3}\Pi$ states dissociating into $4s(\mathrm{K})+5p(\mathrm{Rb})$ and the $3\,^{1,3}\Sigma^+$ and $2\,^{1,3}\Pi$ states dissociating into $4p(\mathrm{K})+5s(\mathrm{Rb})$ are reported in Table II and Fig. 1. The $2,3\,^{1,3}\Sigma^+$ and $1,2\,^{3}\Pi$ pair states show large splittings in energy. Their wave functions at short and intermediate internuclear distances showed mixtures in large extent of those two atomic characters.

However, the $\underline{1}$, $\underline{2}$ pair states show a small splitting in potential energy. The vibrational energy levels of these two states are reported in Fig. 2. These vibrational energy levels are quite irregular. The lowest vibrational energy levels of the $\underline{1}$ state are $G(0)=21$, $G(1)=50$, $G(2)=75$, $G(3)=98$, $G(4)=120$, and $G(5)=144$ cm^{-1} and those of the $\underline{2}$ state are $G(0)=31$, $G(1)=89$, $G(2)=144$, $G(3)=203$, $G(4)=262$, and $G(5)=321$ cm^{-1}. The Dunham-type analyses for these states are rather meaningless. The small splitting of the potential-energy curves for these states over a wide range of internuclear distances implies a weak coupling between these two states. The nonadiabatic correction (see Sec. II) proved to be so small [the diagonal ($m=n$) and coupling ($m\neq n$) terms being less than 10^{-5}] that it could be neglected. This means that vibrations do not mix these two adiabatic electronic states.

The molecular spectroscopic constants are listed in Table III. Dunham analysis for the $2\,^{3}\Pi$ state did not converge because of its extremely shallow potential-energy well. The CI wave functions analyzed in terms of the atomic-orbital (AO) populations in Figs. 3(a) and 3(b) clearly show the complementary nature of these two $^{1}\Pi$ states. The $\underline{1}$ state is essentially composed of the s AO of potassium and the p_π AO of rubidium, while the $\overline{2}$ state is essentially composed of the s AO of rubidium and the p_π AO of potassium. At $R\leq 8$ bohrs and $R\cong 13$ bohrs, however, there occurs substantial mixing between these two basis components.

In contrast, the $2,3\,^{1,3}\Sigma^+$ and $1,2\,^{3}\Pi$ states show mixtures in larger extend (approximately half and half) of the $4s(\mathrm{K})+5p(\mathrm{Rb})$ and $4p(\mathrm{K})+5s(\mathrm{Rb})$ characters and the AO populations change rather monotonously as a function of the internuclear distance (see Fig. 4).

To understand the strange behavior of the $\overline{1}$ and $\overline{2}$ states, one configuration state function (CSF) valence-band (VB) description for these states, i.e., the nonorthogonal $|4s5p_\pi\rangle$ and $|5s4p_\pi\rangle$ states, was analyzed. Then the coupling between those states $\langle 4s5p_\pi|H|5s4p_\pi\rangle$ reduces to a single integral $\langle 4s(1)5p_\pi(2)|r_{12}^{-1}|5s(1)4p_\pi(2)\rangle$. That integral varies as

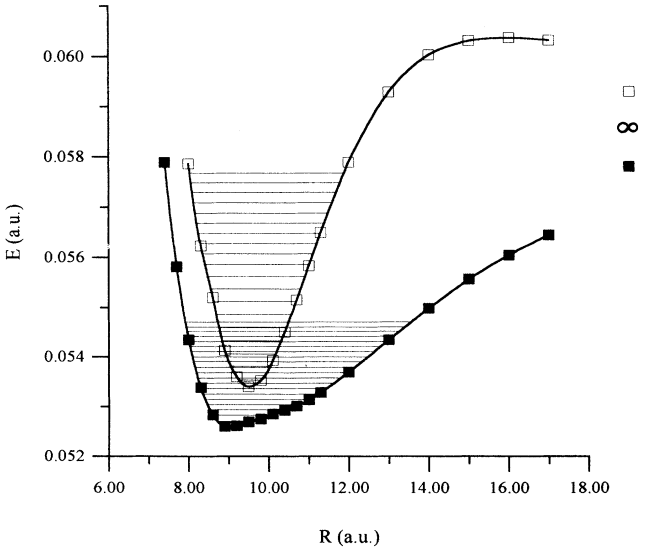

FIG. 2. Potential-energy curves and vibrational energy levels of the 1 and $2\,^{1}\Pi$ states.

TABLE III. Molecular spectroscopic constants.

States	T_e[a] (cm^{-1})	ω_e (cm^{-1})	R_e (pm)
$1\,^{1}\Sigma^+$	−3 792	65	405
$2\,^{1}\Sigma^+$	7 066	53	502
$3\,^{1}\Sigma^+$	10 322	34	549
$1\,^{1}\Pi$	11 430	22[b]	504
$2\,^{1}\Pi$	11 690	59[b]	478
$2\,^{3}\Sigma^+$	9 220	47	522
$3\,^{3}\Sigma^+$	14 316	62	473
$1\,^{3}\Pi_0$	5 951	69	426
$1\,^{3}\Pi_1$	6 012	69	426
$1\,^{3}\Pi_2$	6 073	69	426
$2\,^{3}\Pi_0$	12 886	c	511
$2\,^{3}\Pi_1$	12 940	c	511
$2\,^{3}\Pi_2$	12 994	c	511

[a]With respect to the energy of $\mathrm{K}(4s)+\mathrm{Rb}(5s)$.
[b]See the text for the $G_{(v)}$ values.
[c]Dunham's analysis did not converge.

0.025 33, 0.020 49, 0.015 20, 0.008 70, 0.004 77, 0.002 70, and 0.001 40 (in hartree) at 3, 5, 7, 10, 13, 16, and 20 bohrs, respectively. In two-states approximation, the adiabatic electronic states $|\Phi_1\rangle$ and $|\Phi_2\rangle$ can be written as

$$|\Phi_1\rangle = c|4s5p_\pi\rangle + d|5s4p_\pi\rangle ,$$

$$|\Phi_2\rangle = -d|4s5p_\pi\rangle + c|5s4p_\pi\rangle .$$

The angle defined by $\varphi = -\arctan(d/c)$ varies as 51°, 44°, 41°, 39°, 34°, 27°, and 18° at 3, 5, 7, 10, 13, 16, and 20 bohrs, respectively. It shows the coupling between $|4s5p_\pi\rangle$ and $|5s4p_\pi\rangle$ becoming progressively stronger as the two atoms approach each other. That seems quite contrary to the population analysis. One answer to that disagreement may be found in the inadequacy of representing each of the 1 and 2 states by a single VB CSF. A qualitatively identical conclusion is reached when the effective Hamiltonian [12] and the perturbation method up to the second order are used. We are unable to give here a plausible explanation for this strange character of the 1 and 2 states.

The dipole moment functions in Fig. 3(c) show that the 1 state is $K^{\delta+}Rb^{\delta-}$, while the 2 state is $K^{\delta-}Rb^{\delta+}$ for a wide range of internuclear distances. This is parallel to the analysis of the total populations (the net charge of ei-

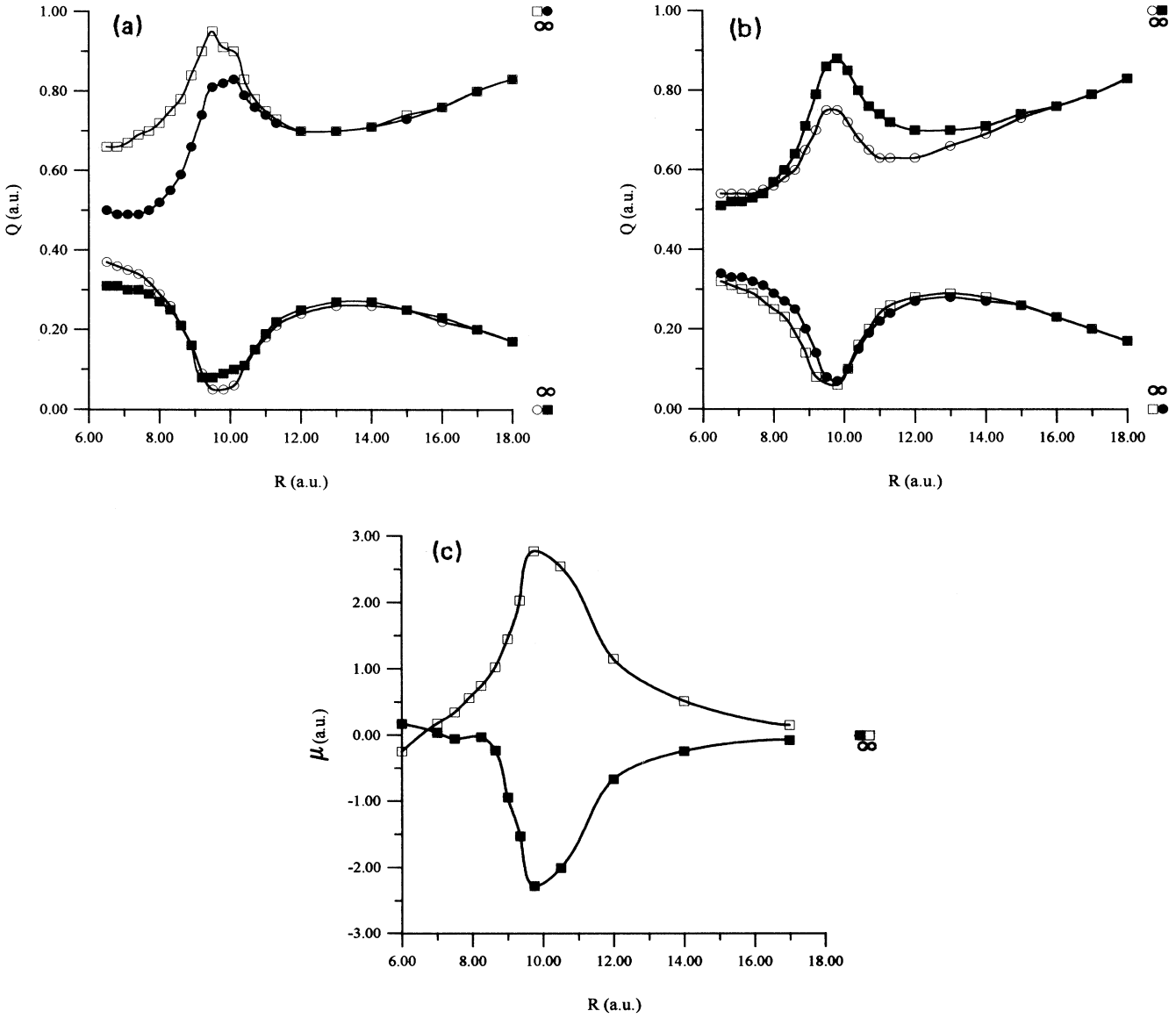

FIG. 3. (a) Population analysis of the wave functions for the 1 $^1\Pi$ state and the 2$^1\Pi$ state: filled circle, s(K); filled square, p_π(K); empty circle, s(Rb); empty square, p_π(Rb). (b) Population analysis of the wave functions for the 2 $^1\Pi$ state: same as in (a). (c) Dipole moment curves of the 1 $^1\Pi$ (filled square) and the 2 $^1\Pi$ (empty square).

ther atom is very small). The transition dipole moments $\underline{1}$-X and $\underline{2}$-X, shown as functions of the internuclear distance in Fig. 5, exhibit remarkably contrasting behavior. As the ground state is principally made of $4s(\mathrm{K})+5s(\mathrm{Rb})$, the $\underline{1}$-X and $\underline{2}$-X transition dipole moments can be decomposed into $4s(\mathrm{K})\rightarrow 4p_\pi(\mathrm{K})$, $5s(\mathrm{Rb})\rightarrow 5p_\pi(\mathrm{Rb})$, and other minor terms. The $\langle 4s(\mathrm{K})|er_i|4p_i(\mathrm{K})\rangle$ is 3.215 a.u. and the $\langle 5s(\mathrm{Rb})|er_i|5p_i(\mathrm{Rb})\rangle$ is 3.396 a.u. The largest contributions among the minor terms are the cross integrals $\langle 4s(\mathrm{K})|er_i|5p_i(\mathrm{Rb})\rangle$ and $\langle 5s(\mathrm{Rb})|er_i|4p_i(\mathrm{K})\rangle$. These are about $\frac{1}{3}$ of the major terms at $R=10$ bohrs and about $\frac{1}{10}$ at $R=15$ bohrs. Due to a destructive combination of these terms with opposite relative phases, the $\underline{2}$-X transition dipole moment is practically zero at short internuclear distances. It increases in the weakly coupled region, then remains nearly constant at longer internuclear distances, and finally converges to the $4s(\mathrm{K})$-$4p(\mathrm{K})$ value at long distances. In contrast, the $\underline{1}$-X transition dipole moment has relatively large values at short internuclear distances, then decreases in the weakly coupled region, and then slowly converges to the $5s(\mathrm{Rb})$-$5p(\mathrm{Rb})$ value at very long (not appearing in Fig. 5) distances due to a much more diffuse nature of the $5p$ AO in comparison with that of $4p$.

The Einstein coefficients for the vibronic transitions $v'\rightarrow v''$, where v' belongs to $\underline{1}$ or $\underline{2}$ states and v'' belongs to the $X\,^1\Sigma^+$ state, are reported in Fig. 6. This figure shows an unusual characteristic of these transitions. Indeed, both types of transition appear to have significant intensity for a wide range of $\Delta v=v'-v''$. The resolution of the (ro)vibronic transition spectra between the X state and the $\underline{1}$ and $\underline{2}$ states may seem extremely complicated due to the proximity of these two states, even though the ΔG_v values of the $\underline{1}$ and $\underline{2}$ states are quite different. Nevertheless, the two types of transition, $\underline{1}$-X and $\underline{2}$-X differ in a very striking way. The $\underline{1}$-X transition has significant intensities for transitions from or to low $v''(X)$ vibrational states, except $v''=0-5$. In contrast, the $\underline{2}$-X transition probabilities from or to low-$v''(X)$ vibrational states are negligible. This is due to different behavior of the two transition dipole moments as functions of internuclear distance (Fig. 5) and the vibrational wave functions of the ground state (Franck-Condon principle), which are concentrated around 7.688 bohrs. It is worth noticing the contrasting patterns between Figs. 6(a) and 6(b) and the presence of a series of belts (set of high-intensity bands) in Fig. 6(a). As a consequence, the most intense bands for

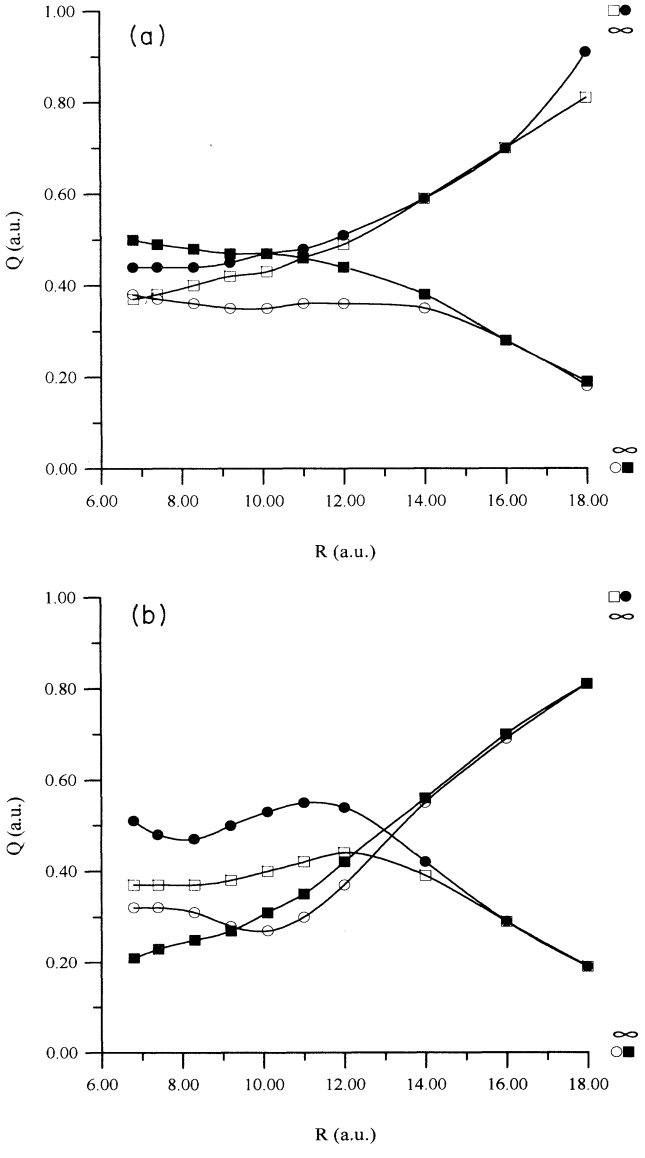

FIG. 4. Population analysis of the wave function for (a) the $1\,^3\Pi$ state and (b) the $2\,^3\Pi$ state: filled circle, $s(\mathrm{K})$; filled square, $p_\pi(\mathrm{K})$; empty circle, $s(\mathrm{Rb})$; empty square, $p_\pi(\mathrm{Rb})$.

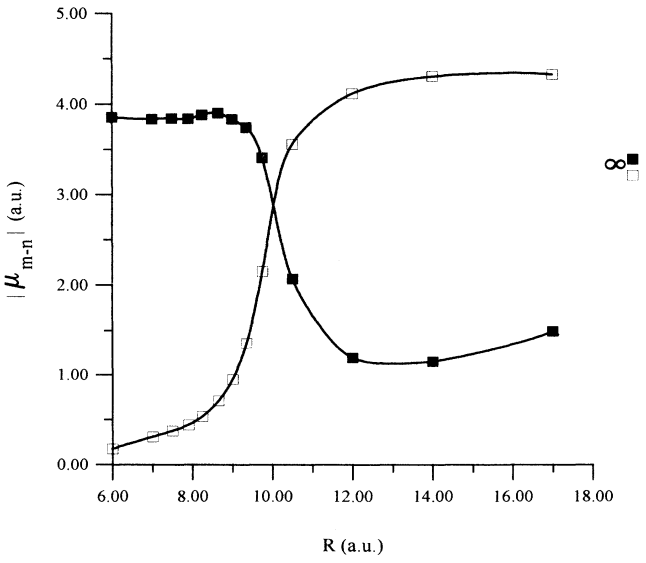

FIG. 5. Transition dipole moment curves: $1\,^1\Pi-X$, filled square; $2\,^1\Pi-X$, empty square.

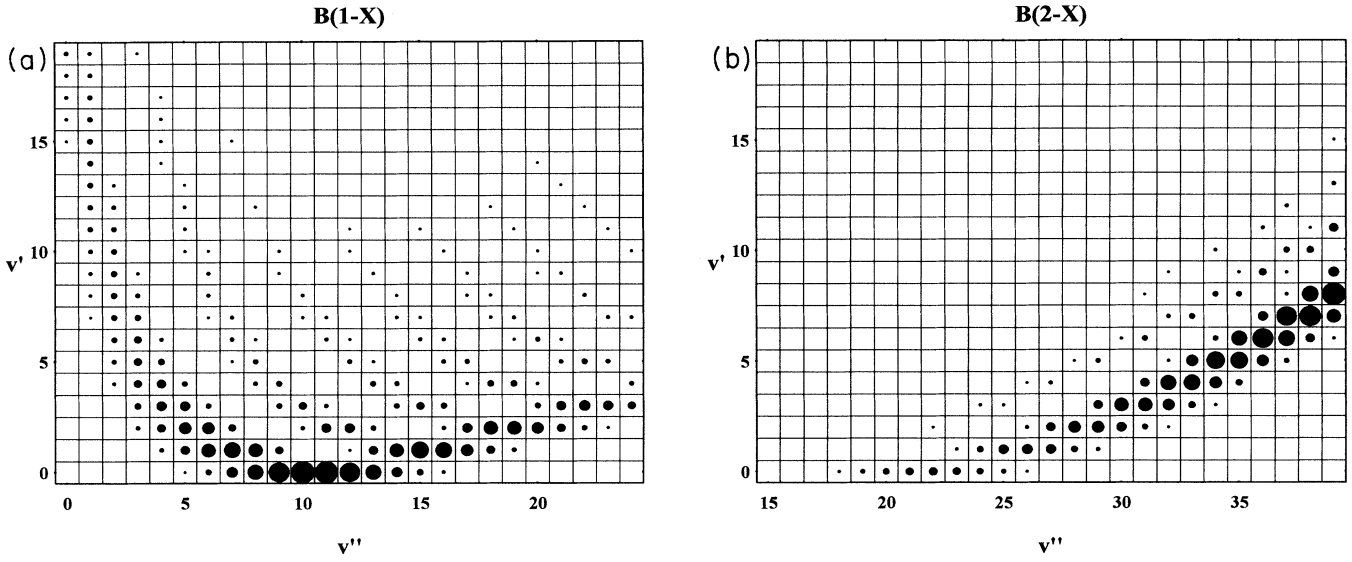

FIG. 6. Einstein coefficients for stimulated emission in $J^{-1}\,m^3\,s^{-2}$: (a) $1\,^1\Pi-X$, the largest dot represents 2.51×10^{20} and the smallest represents 0.302×10^{20}; (b) $2\,^1\Pi-X$, coefficients vary from 2.12×10^{20} to 0.254×10^{20}.

the 2-X transitions appear in longer wavelengths than those of the most intense 1-X transitions, contrary to the order of T_e's for these states [13].

Considering limitations of the present calculation, our 2-1 transition energies may be off by up to 300 cm^{-1} with respect to the real values. However, we believe that the qualitative conclusion regarding the 1-X and 2-X transition intensities remains valid. Unfortunately, no experimental data are available to verify this.

ACKNOWLEDGMENTS

The calculation presented in this work was done with the IBM-3090 machine of the CCSC near Strasbourg and the CRAY-2 machine of the CCVR at Palaiseau through a grant from the CNRS. Many interesting discussions with Dr. Amanda Ross are gratefully acknowledged. Laboratoire de Chimie Quantique is UPR-193 of the CNRS.

[1] A. J. Ross, C. Effantin, P. Crozet, and E. Boursey, J. Phys. B **23**, L247 (1990).
[2] R. Beuc, S. Milosevic, and G. Pichler, J. Phys. B **17**, 739 (1984).
[3] C. E. Moore, *Atomic Energy Levels*, Natl. Bur. Stand. (U.S.) Circ. No. 467 (U.S. GPO, Washington, DC, 1971), Vols. 1–3.
[4] M. M. Hurley, L. F. Pacios, P. A. Christiansen, R. B. Ross, and W. C. Ermler, J. Chem. Phys. **84**, 6840 (1986).
[5] L. A. LaJohn, P. A. Christiansen, R. B. Ross, T. Atashroo, and W. C. Ermler, J. Chem. Phys. **87**, 2812 (1987).
[6] M.-M. Rohmer, R. Ernenwein, M. Ulmschneider, R. Wiest, and M. Bénard, Int. J. Quantum Chem. **40**, 723 (1991); T. Leininger, G. H. Jeung, M. M. Rohmer, and M. Pélissier, Chem. Phys. Lett. **190**, 342 (1992).
[7] B. R. Brooks and H. F. Schaefer III, J. Chem. Phys. **70**, 5092 (1979).
[8] P. E. M. Siegbahn, J. Chem. Phys. **72**, 1647 (1980).
[9] S. R. Langhoff and E. R. Davidson, Int. J. Quantum Chem. **8**, 61 (1974).
[10] J. G. Eaton, H. W. Sarkas, S. T. Arnold, K. M. McHugh, and K. H. Bowen, Chem. Phys. Lett. **193**, 141 (1992).
[11] E. Durand, *Mécanique Quantique* (Masson, Paris, 1970), Vol. 1, pp. 572–576.
[12] G. Nicolas and P. Durand, J. Chem. Phys. **72**, 453 (1980).
[13] A. Yiannopoulou, T. Leininger, A. M. Lyyra, and G.-H. Jeung, Int. J. Quantum Chem. (to be published).